

ABOUT COMPUTATIONS OF HELE-SHAW FLOW OF NON-NEWTONIAN FLUIDS

L. KONDIC*, P. FAST**, and M. J. SHELLEY**

*Departments of Mathematics and Physics, Duke University, Durham, NC 27708,
kondic@math.duke.edu

**Courant Institute, New York University, New York, NY 10012

ABSTRACT

The flow of a fluid confined between two solid plates (Hele-Shaw cell) is of considerable interest in a variety of applications. Further interest in two phase flow in this geometry stems from the close analogy between the dynamics of fluid-fluid interface and the propagation of the solidification front. While the flow of Newtonian fluids is rather well understood, it is much more complicated to compute flows of non-Newtonian fluids. We find that the dense-branching morphology of Newtonian liquids may be replaced by dendritic fingers with stable tips and sidebranches, and discuss resulting length scales.

INTRODUCTION

Flows of complex, non-Newtonian fluids are of considerable technological importance. In particular confined thin-gap flows of non-Newtonian fluids are relevant to industrial processes such as injection molding or display device design [1]. A two-phase flow in this setting is a scientifically important one, given the close analogy between the Saffman-Taylor instability of driven Newtonian fluid with quasi-static solidification (and the Mullins-Sekerka instability [2]), electrochemical deposition [3], and many other physical problems.

In this work, we concentrate on the interfacial dynamics of a gas bubble expanding into fluid in a radial Hele-Shaw cell (see Fig. 1). When the fluid is Newtonian, a dense branching pattern morphology is observed [4], as the outcome of the nonlinear development of the Saffman-Taylor instability. It is characterized by tip-splitting of the interface and the formation of branched structures. On the other hand, experiments performed with complex liquids such as liquid crystals [5], polymer solutions and melts [4], clays [6], and foams [7], have shown that the structures reminiscent of solidification ones - dendritic fingers, side branching, can be induced in these fluids. One property shared by these different liquids is that they are shear thinning, and we will concentrate on this property. Elastic response of the fluid can also be an important effect, though we will not consider it here.

We start from the generalized Darcy's law governing the bulk fluid flow [8]. Combined with appropriate boundary conditions, this yields a nonlinear, elliptic boundary value problem (BVP) for the pressure in the driven fluid. Fully nonlinear, time dependent simulations of a bubble growing into a shear thinning fluid show that shear thinning influences considerably the evolution of the interface, and in agreement with experiments, can lead to the formation of fingers which do not split, and can resemble the dendritic structures observed in solidification.

In this paper we give an outline of our methods, combined with new results related to experimentally measurable quantities, such as observed length scales and the finger velocity. The reader is referred to [8, 9] for the formulation of a Darcy's law, and more detailed explanation of the role which shear thinning plays in pattern formation, and to [10] for the relation of the model employed here to more general viscoelastic fluid models.

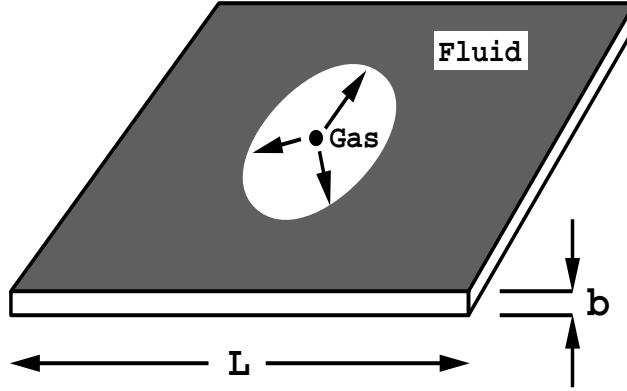


Figure 1: Hele-Shaw cell

THEORY

Darcy's law for a non-Newtonian fluid

We use the fluid model in which non-Newtonian character of fluid enters through rate-of-strain dependence of the fluid viscosity

$$\rho \frac{D\mathbf{v}}{Dt} = -\nabla p + \nabla \cdot (\mu(|\mathbf{S}|^2)\mathbf{S}), \quad \nabla \cdot \mathbf{v} = 0, \quad (1)$$

where \mathbf{S} is the rate-of-strain tensor, and $|\mathbf{S}|^2 = \text{tr}(\mathbf{S}^2) = \sum_{ij} S_{ij}^2$. The viscosity is taken to be given by $\mu(|\mathbf{S}|^2) = \mu_0(1 + \alpha\tau^2|\mathbf{S}|^2)/(1 + \tau^2|\mathbf{S}|^2)$. Here τ is the relaxation time of the fluid, μ_0 its zero shear rate viscosity, and α measures shear dependence: $\alpha = 1$ gives Newtonian response, $\alpha > 1$ gives shear thickening, and $\alpha < 1$ shear thinning. In practice, most non-Newtonian fluids are shear thinning, and we concentrate on this case.

The flow in a Hele-Shaw geometry is significantly simplified by the small aspect ratio $\epsilon = b/L \ll 1$. The Reynolds number is small, so that inertial terms could be neglected, and the velocity gradients in the short, z , direction are much larger than the lateral ones. Keeping only the terms of $O(\epsilon)$, and averaging over the gap width, one obtains a generalized Darcy's law applicable to a shear thinning fluid (the choice of appropriate sales is discussed in [8, 9])

$$\mathbf{u} = -\frac{1}{12 \bar{\mu}_\alpha(We^2|\nabla p|^2)} \nabla p, \quad \text{and} \quad \nabla \cdot \mathbf{u} = 0, \quad (2)$$

where ∇ is the lateral gradient operator, and \mathbf{u} is gap averaged fluid velocity. Weissenberg number, $We = \tau/\tau_{flow}$, measures the ratio of the time scale of the fluid, τ , and the relevant time scale imposed by flow, τ_{flow} . The viscosity $\bar{\mu}_\alpha(We^2|\nabla p|^2)$ is constructed from μ and shares its monotonicity properties, i.e., if the fluid is shear thinning then $\bar{\mu}_\alpha(We^2|\nabla p|^2)$ decreases monotonically with increasing argument [8].

Expanding bubble problem

Now we apply the resulting equations to the problem of an air bubble expanding into a non-Newtonian fluid. Additional nondimensional parameter, capillary number (Ca), which measures the ratio of capillary to viscous forces, enters through imposed Laplace-Young boundary conditions. To facilitate comparison with experiments (see [4] and references

therein), we define Ca and We

$$Ca = \frac{12\mu_0\dot{R}_0 R_0^2}{\gamma b^2}, \quad \text{and } We = \frac{\tau\dot{R}_0}{b}, \quad (3)$$

where it is assumed that all the quantities can be varied *independently*. The lateral length scale is chosen as the initial radius of the bubble, R_0 , and the velocity scale is the initial bubble velocity, \dot{R}_0 . At the boundaries, the pressure jump $[p]$ is given by $[p] = Ca^{-1}\kappa$ for the pressure jump $[p]$, where κ is the lateral curvature. A nonlinear BVP for the pressure follows [9]

$$\nabla \cdot \left(\frac{\nabla p}{\bar{\mu}_\alpha (We^2 |\nabla p|^2)} \right) = 0, \quad p|_{\Gamma_i} = 1 - \frac{\kappa_i}{Ca}, \quad p|_{\Gamma_e} = \frac{\kappa_e}{Ca}, \quad (4)$$

where $,_{i,e}$ stand for the internal and external fluid boundaries. The motion of the interfaces follows from the requirement that they move with local fluid velocities.

Numerical methods

The full evolution problem, Eq. (4), is much harder to solve than the corresponding problem for a Newtonian fluid, where the pressure is harmonic. In the non-Newtonian case, p satisfies the nonlinear BVP, Eq. (4), and must be solved for in the whole domain. Since the problem is driven by the curvature of the boundaries, high spatial resolution is required.

To solve for the pressure, we use a Lagrangian grid which conforms to the interfaces and moves with the fluid. Once the pressure is obtained, velocity of the fluid (and of the boundaries) is obtained using Darcy's law, Eq. (2). As initial data, we take the interior interface $,_i$ as a circle perturbed with a single azimuthal mode $m = 4$, and the outer boundary $,_e$ as a circle. For efficiency, we impose a four-fold symmetry on the initial bubble shape, and the solution. More details about computational methods are given in [9, 10].

RESULTS

The effect of shear thinning on the dynamics of the interface

Figure 2 shows the simulation of an expanding bubble for Newtonian and non-Newtonian fluid, plotted at equal time intervals. In Fig. 2a we observe typical pattern formation for a Newtonian fluid, where the unstable mode is growing into a petal, which widens, and then splits into two as its radius of curvature increases, in agreement with linear theory [11]. The bubble evolution in a strongly shear thinning fluid is strikingly different, as is illustrated in Fig. 2b. The effect of shear thinning is to suppress the tip splitting of the outwardly growing petal. As the petal expands outwards, it appears to near a splitting, but then “refocuses”, leaving behind “side-branches”, and continues to grow outwards.

In [9] it is shown that the lowest viscosity appears at the ends of the petals, and then increases sharply as one moves away from the tips, and is highest within the fjords, where it is nearly unity (the “zero shear” viscosity is normalized to one). It is this phenomena that results in the narrowed petals: shear thinning effect increases the local fluid velocity at the tips. This effect is limited by capillarity, which seeks to lower the length to area ratio, and which is also likely related to the production of “side branches” left behind the advancing tip.

There are three (nondimensional) parameters which determine the dynamics of the interface: Ca , which measures the relative strength of surface tension and viscous forces, and

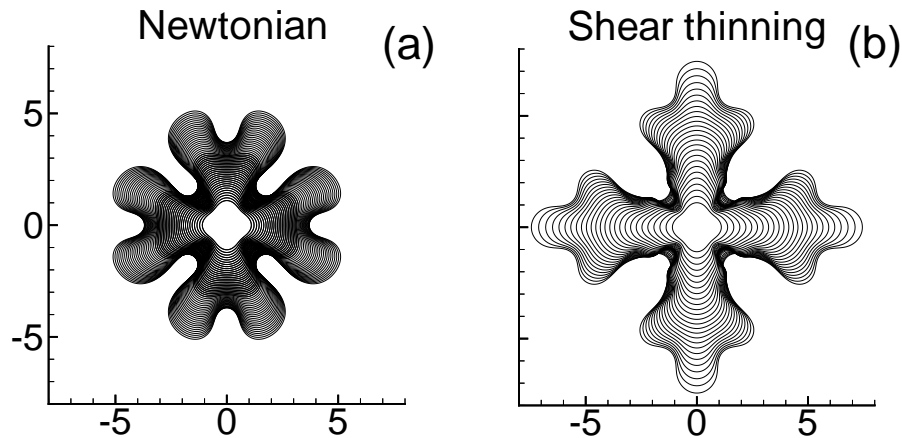


Figure 2: The snap-shots of the evolving bubble interface for (a) Newtonian fluid and (b) strongly shear thinning fluid ($Ca = 480$ for both simulations, $\alpha = 0.15$, $We = 0.15$ for shear thinning one).

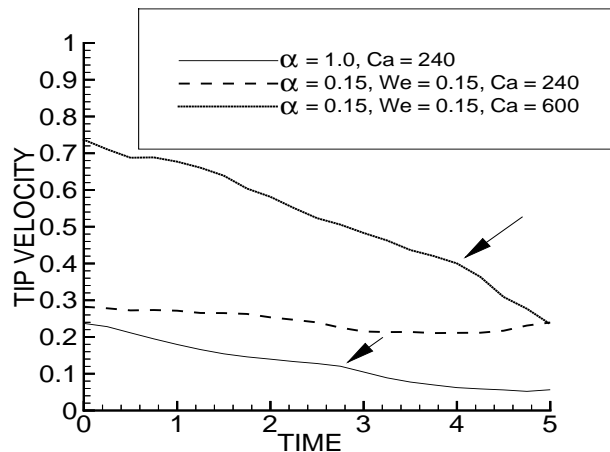


Figure 3: The velocity of tip propagation. Solid lines show tips which split; broken line shows non tip-splitting finger. The arrows show the point where curvature of the tip changes sign.

We and α , which determine shear thinning properties of the fluid. Flows characterized by some combination of these parameters lead to the formation of fingers whose tips do not split (as shown in Fig. 2b); different parameters might lead to production of tip splitting petals, resembling the patterns characteristic for a Newtonian fluid. Detailed discussion of the influence which shear thinning character of the fluid has on the pattern formation, as well as detailed parametric dependence of the observed patterns, are given in [9, 10].

Another effect of shear thinning is to modify the velocity of advancing fingers/petals. Figure 3 shows the tip velocity for a Newtonian fluid, and for two choices of parameters characterizing shear thinning fluids; the latter two differ only in Ca . The choice $Ca = 240$ leads to formation of fingers which do not split, and is characterized by the tip velocity which is approximately constant. The other choice, $Ca = 600$, leads to a tip splitting petal, whose velocity is continuously decreasing. This effect has been noted in the theoretical work [15], where the curvature of the finger tip was held constant artificially.

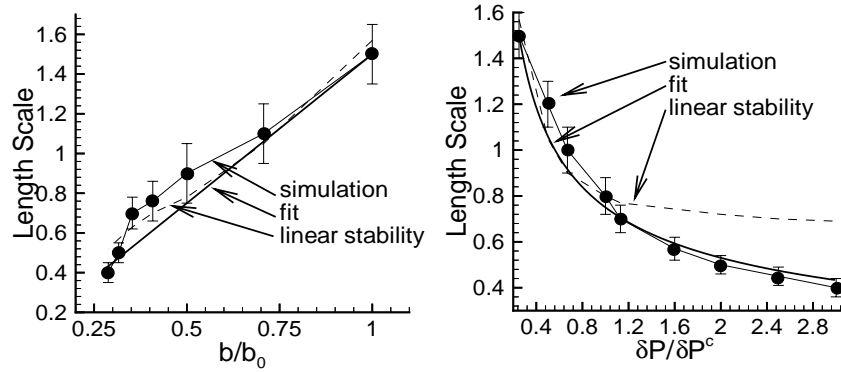


Figure 4: The dependence of the length-scale l on plate separation b (a), and driving pressure δP (b). Here b_0 (a) and δP^c (b) are the plate separation and the driving pressure which give $Ca = 240$ and $We = 0.15$. Linear stability results (dashed) [9, 10], simulation results (dots) and fits $l = kb$ (a), and $l \sim k'(\delta P/\delta P^c)^{-1/2}$ (b) (solid) are shown. The constants k , k' are determined from the data points $b = b_0$ (a), and $\delta P = \delta P^c$ (b) ($\alpha = 0.15$).

Emerging length-scales

A typical length-scale (l) of the patterns which develop in a radial Hele-Shaw flow for Newtonian fluids is determined by a single parameter, the capillary number Ca . For large Ca , linear stability suggests that a length-scales associated with the initial growth of the patterns is given by $\lambda_m \approx 2\pi R\sqrt{3/Ca}$ [11], where λ_m is the wavelength of the most unstable mode, and R is the time-dependent radius of the expanding bubble. We look into our simulation results for a similar length scaling in shear thinning fluids.

In experiments [12], emerging length-scales have been measured as the gap width b is varied. These results suggest that the length-scale scales roughly linearly with b . For Newtonian fluids this observation confirms the result of linear stability, since $Ca \sim 1/b^2$ if the characteristic velocity is fixed independently of b . However, the flow also depends up the Weissenberg number, We , which is itself a function of b . So, one should modify both Ca and We in order to obtain realistic comparison with experimental results. These resulting length-scales are given in Fig. 3a. While it is not obvious that scaling $l \sim b$ is satisfied, there is a good qualitative agreement of the simulations and the experimental results.

The driving pressure is another control parameter whose influence on emerging length scales can be explored. In experiments [6, 13] increasing the driving pressure typically decreases the observed length scales. Figure 3b compares the length scales obtained from our simulations to the results of linear stability [9, 10], and to a fitting function of the form $l \sim 1/\sqrt{\delta P}$, where δP is the driving pressure. The motivation for this particular fit arises from analogy with Newtonian fluids where $l \sim 1/\sqrt{Ca}$, and $Ca \sim \delta P$. Here we observe that linear stability theory and simulational results agree rather well at smaller driving pressures. For larger values of δP , the length-scales resulting from linear stability analysis saturate to a constant, while the results of the simulations fit $l \sim 1/\sqrt{\delta P}$ very closely. We hope to verify this prediction experimentally [14].

CONCLUSION

In this paper we have shown that, under certain assumptions, flow in a Hele-Shaw cell of a complex viscoelastic fluid simplifies to that of a generalized Newtonian fluid. Full numerical simulations of the two phase (liquid/gas) flow show that shear thinning behavior of the driven fluid modifies significantly the morphology of the patterns, relative to those for Newtonian liquids, by suppressing tip-splitting. Furthermore, the varying of length scales emerging from our simulations, as parameters are changed, is in good qualitative agreement with those observed in experiments. In particular, we observe in our simulations that the typical length scale of the patterns scales with driving pressure as $l \sim \delta P^{-1/2}$. This prediction, which is of considerable importance in technological processes such as injection molding or oil recovery is still to be verified experimentally.

We are continuing our work in few directions: improvement in numerical methods, formulation of more realistic boundary conditions, and extension of our model to the fluids characterized with different rheological properties. By combining experimental, theoretical and computational efforts, we hope to further contribute to the understanding of complex fluids and pattern formation.

ACKNOWLEDGMENTS

This work was supported in part by DOE Grant No. DE-FG02-88ER25053, NSF Grants No. DMR-9321792 and DMS95-04577, and by ONR Grant No. N00014-96-1-0656.

References

- [1] C. A. Hieber, in A. I. Isayev, ed., *Injection and Compression Molding Fundamentals*. Marcel Dekker, New York, 1987; C. Z. Van Doorn, *J. Appl. Phys.* **46**, 3738 (1975).
- [2] J. S. Langer, in H. E. Stanley, ed. *Statistical Physics*. North-Holland, 1986.
- [3] J. Bockris and A. Reddy, *Modern Electrochemistry*, Plenum Press, 1970.
- [4] K.V. McCloud and J. V. Maher, *Phys. Rep.* **260**, 139 (1995).
- [5] A. Buka, P. Palffy-Muhoray, and Z. Racz, *Phys. Rev. A* **36**, 3984 (1987).
- [6] H. Van Damme and E. Lemaire, in J.C. Charmet, S. Roux, and E. Guyon, editors, *Disorder and Fracture*, page 83. Plenum Press, New York, 1990.
- [7] S. S. Park and D. J. Durian, *Phys. Rev. Lett.* **72**, 3347 (1994).
- [8] L. Kondic, P. Palffy-Muhoray, and M. J. Shelley, *Phys. Rev. E* **54**, 4536 (1996).
- [9] L. Kondic, M. J. Shelley, and P. Palffy-Muhoray, *Phys. Rev. Lett.* **80**, 1433 (1998).
- [10] P. Fast, L. Kondic, M. J. Shelley, and P. Palffy-Muhoray, in preparation, 1998.
- [11] L. Paterson, *J. Fluid Mech.* **113**, 513 (1981).
- [12] G. Daccord and J. Nittmann, *Phys. Rev. Lett.* **56**, 336 (1986).
- [13] M. Kawaguchi, K. Makino, and T. Kato, *Physica D* **105**, 121 (1997).
- [14] P. Palffy-Muhoray, R. Ennis, M. J. Shelley, and L. Kondic, in preparation, 1998.
- [15] E. Meiburg and G. M. Homsy, *Phys. Fluids* **31**, 429 (1988).